Available online at www.sciencedirect.com

SciVerse ScienceDirect

Solar Energy 86 (2012) 541–547

SOLAR ENERGY

www.elsevier.com/locate/solener

Effective conversion efficiency enhancement of solar cell using ZnO/PS antireflection coating layers

Khaldun A. Salman *, Khalid Omar, Z. Hassan

Nano-Optoelectronics Research and Technology Laboratory, School of Physics, University Sains Malaysia, Penang 11800, Malaysia

Received 13 July 2011; received in revised form 14 October 2011; accepted 29 October 2011
Available online 3 December 2011

Communicated by: Associate Editor Takhir Razykov

Abstract

Zinc oxide (ZnO) film was deposited on a porous silicon (PS) layer using a radio frequency sputtering system while the PS layer was prepared by a photoelectrochemical etching method. The ZnO/PS layers were found to be an excellent antireflection coating (ARC), exhibiting exceptional light trapping at wavelengths ranging from 400 to 1000 nm because of their lowest effective reflectance. This, in turn, leads to increase the efficiency of solar cell to 18.15%. The ZnO film was highly oriented with the *c*-axis perpendicular to the PS layer. The average crystallite size of the PS and ZnO/PS layers were 17.06 and 17.94 nm, respectively. Photoluminescence emission peaks proved the nanocrystalline characteristic of the PS layer and the ZnO film. Raman measurements of the ZnO/PS layers were determined at room temperature and indicate that a high-quality ZnO nanocrystalline film was formed. In the current paper, ZnO/PS ARC layers are attractive and offer a promising technique to produce high-efficiency, low-cost solar cells.

Keywords: Efficiency; Solar cell; Zinc oxide; Porous silicon; Anti-reflection coating

1. Introduction

A porous silicon (PS) layer formed on a crystalline silicon (c-Si) wafer using electrochemical etching exhibits photoluminescent and electroluminescent properties similar to those of semiconductors with a direct energy band gap (Canham, 1990). The main improvement in the performance of the PS layers is the rough surface and low effective refractive index compared with c-Si, which can decrease the reflective loss of solar radiation and lead to an increase of approximately 15–20% of the short-circuit current density (J_{sc}) of solar cells (Yae et al., 2006; Vitanov et al., 1997; Ueda et al., 1988). PS layers have become an attractive material for solar cells because of their band gap broadening, wide optical transmission ranging from 700 to 1000 nm, and surface roughness (Koshida and Koyama, 1992). PS layers are an excellent antireflection coating (ARC) for solar cells (Ben Ranha and Bessais, 2010). The ARC can enhance the efficiency of solar cells by increasing light trapping in the active region (Yoo, 2010; San Vicente et al., 2011).

In the last couple of years, many researchers have increasingly focused on zinc oxide (ZnO) because of its multiple applications, such as laser diodes (Ye et al., 2007), transparent conductive contacts (Wong and Searson, 1999), and solar cells (Bahadur et al., 1986; Sil and Chakrabarti, 2010; Lu et al., 2010). ZnO has a direct band gap (3.37 eV), a high exciton binding energy (60 meV) at room temperature (RT), and a wurtzite crystal structure (Pawar et al., 2011). Recently, ZnO has attracted attention as one of the materials for the ARC of solar cells because it has good transparency and an appropriate refractive index (Yun-Ju et al., 2008; Kawakami et al., 2003; Kim and Kim, 2003; Liu et al., 2001; Greene et al., 2005; Tak and Yong, 2005; Chen and Gao, 2006; Riaz

* Corresponding author. Tel.: +60 175373031; fax: +60 46579150.
E-mail address: khaldunphysics@gmail.com (K.A. Salman).

0038-092X/$ - see front matter © 2011 Elsevier Ltd. All rights reserved.
doi:10.1016/j.solener.2011.10.030

et al., 2009; Chen and Sun, 2010b). The integration of ZnO films and c-Si samples is important. However, the deposition of high-quality ZnO films on c-Si samples introduces stress between the materials because of the large mismatch in lattice constants and thermal expansion coefficients (Hsu et al., 2005). Despite these problems, ZnO thin films have been successfully deposited on spherical solar cells as an ARC with an efficiency of 11.8% (Minemoto et al., 2007).

The PS layer is a convenient material for accommodating the deposition of ZnO film onto pores in the layer because the PS layer has a large internal surface area, high resistance, and strong absorbability (Bisi et al., 2000). The integration of ZnO films and a PS layer is more important because the deposition of high-quality ZnO films on a PS layer can introduce a large matching of lattice constants and thermal expansion coefficients (Chen and Sun, 2010b).

Different methods have been proposed to deposit ZnO films on PS layers, such as chemical vapor deposition (Haga et al., 2001), a sol–gel process (Fujihara et al., 2001), direct current sputtering (Harding et al., 1991), and Radio Frequency (RF) sputtering (Cai et al., 2009; Choi et al., 2010; Vasanelli et al., 1987).

In the present work, a ZnO film was deposited on a PS layer using an RF sputtering system, and the PS layer was prepared by the photoelectrochemical etching (PECE) process. The objective of this work was to fabricate a high-efficiency solar cell using the ZnO/PS ARC layer technique.

The authors suggest using ZnO/PS layers as a promising ARC to enhance and increase the light conversion efficiency of solar cells.

2. Experimental

A PS layer was fabricated by PECE process of an n-type c-Si (1 0 0) wafer with a resistivity of 1–20 Ω cm and a thickness of 356–406 μm. Initially, the c-Si wafer was cleaned to remove the oxide layer using the Radio Corporation of America method.

The PECE cell had a circular aperture at the bottom sealed with the c-Si sample. The cell, made of Teflon, was a two-electrode system connected to the c-Si sample as the anode and platinum (Pt) as the cathode (Fig. 1). The c-Si sample was placed in an electrolyte solution HF (48%):C_2H_5OH (98%), 1:4 (by volume) to enable conduction of electrons inside the solution. A current density of 60 mA/cm^2 and an etching time of 20 min were used to prepare the PS layer. Illumination was provided by a 150 W Xenon lamp positioned over the c-Si sample for maximum possible illumination. The synthesis was carried out at RT. Finally, the sample was rinsed in ethanol and air-dried after the etching process.

To fabricate the solar cell, the sample was coated with photoresist. Next, a mask was placed directly above the PS layer and exposed to ultraviolet (UV) radiation for 40 s to form a patterned coating. P-type doping was achieved using the spin coating method by placing boron liquid on the center of the PS layer, followed by spin coating at RT at a speed of 1000 rpm for 10 s. The layer was then placed in a furnace at 100 °C for 15 min to remove moisture. Dopant diffusion was accomplished using a tube furnace at 1000 °C for 60 min under flowing (4 L/min) nitrogen gas.

The 135 nm-thick ZnO film was deposited on the PS layer by RF sputtering with a power of 200 W at ambient temperature using an A500 EDWARDS sputtering unit.

The growth conditions of the ZnO film deposited onto the PS layer are summarized in Table 1.

Annealing of the ZnO/PS layers was done at 500 °C for 30 min under flowing (4 L/min) nitrogen gas.

Annealing improved the quality and optical properties of the ZnO film. Silver evaporation was used on the p-type of the sample to form a metallization grid pattern, and aluminum evaporation was used on the n-type to form a reflector contact. Annealing was carried out at 400 °C for 20 min to insure optimal contact.

Scanning electron microscopy (SEM) and energy dispersive X-ray (EDX) analysis (JSM-6460 LV, Japan) were used to determine the surface morphology and composition of the PS and ZnO/PS layers, respectively. X-ray diffraction (XRD) measurements were carried out using a high-resolution X-ray diffractometer system (PANalytical X'pert

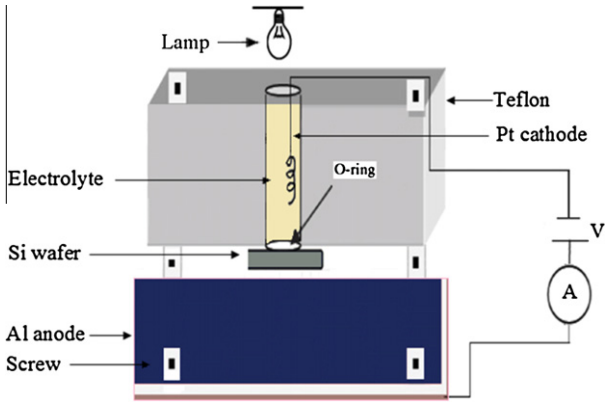

Fig. 1. The photoelectrochemical etching (PECE) cell set up.

Table 1
RF sputtering conditions for ZnO film deposition.

Target	ZnO 99.99%
Target diameter	7.5 cm
Distance between the target and substrate	10 cm
Substrate	PS layer
Substrate temperature	25 °C
Ultimate pressure	1×10^{-6} mbar
Vacuum (plasma) pressure	1.74×10^{-2} mbar
Gas	Ar 99.99%
RF sputtering power	200 W
Deposition rate	Dr_2 0.20 A°s
Deposition time	13 min
The required thickness of ZnO film	135 nm

PRO MRD PW3040, Almelo, The Netherlands) to determine the ZnO crystallite structure using Cu Kα radiation with a wavelength of 0.15406 nm. Photoluminescence (PL) and Raman studies were carried out using a spectroscopy system (Jobin Yvon HR 800 UV, Edison, NJ, USA). Optical reflectance of the c-Si sample, PS, and ZnO/PS layers were obtained using an optical reflectometer (Filmetrics, F20, USA). *I–V* characteristics were studied under the air mass 1.5 global (AM 1.5G) illumination condition (Chen and Sun, 2010a).

3. Results and discussions

Fig. 2 shows the pores randomly distributed on the PS surface. Some pores appeared star-like and had elongated shapes with an average diameter of 6.2 nm, as calculated using the following equation (Ossicini et al., 2003).

$$E(\mathrm{eV}) = E_g + \frac{h^2}{8d^2}\left[\frac{1}{m_e^*} + \frac{1}{m_h^*}\right], \quad (1)$$

where $E(\mathrm{eV}) = 1.81$ eV is the energy band gap of PS obtained from the PL peak of the PS layer as shown in the inset of Fig. 6, $E_g = 1.12$ eV is the energy band gap of c-Si, h is Planck's constant $= 4.13 \times 10^{-15}$ eV s, d is the diameter of the pore, and m_e^* and m_h^* are the electron and hole effective mass, respectively (at 300 K, $m_e^* = 0.19m_o, m_h^* = 0.16m_o$, and $m_o = 9.109 \times 10^{-31}$ kg). Moreover, the surface of the PS layer was etched completely. The formation of numerous, new, tiny pores inside the initial pores and above the pore walls can be clearly distinguished, which increased the porosity (P) of the PS layer to 91% according to the following equation (Hyunwoo et al., 2006):

$$P(\%) = \frac{m_1 - m_2}{m_1 - m_3}, \quad (2)$$

where m_1 and m_2 are the sample weight before and after anodization, respectively; and m_3 is the sample weight after removing the PS layer using a 3% KOH solution in 50 s (Faÿ and Shah, 2008).

The ZnO film was deposited on the PS layer by RF sputtering as shown in the SEM image in Fig. 3. The deposition

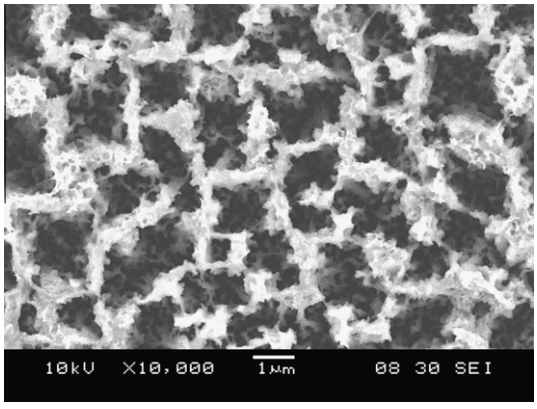

Fig. 2. SEM image of the PS layer.

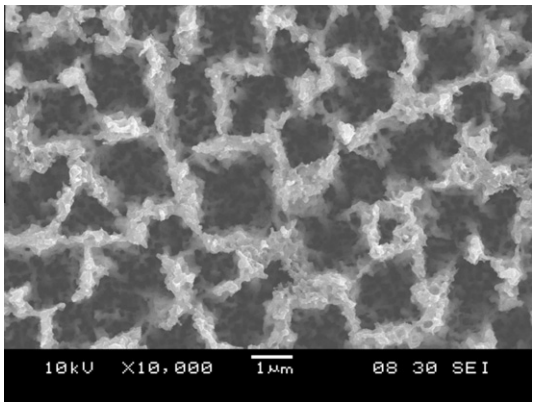

Fig. 3. SEM image of ZnO/PS layers.

of ZnO inside the pores along the walls partially filled or covered the pores.

Fig. 4 shows the EDX spectrum and atomic composition of the ZnO/PS layers. A description of the atomic composition of the elements in the layers is given by the percentage, as shown in the inset table in Fig. 4. The concentrations of these elements are indicated by the peaks, and it is very clear that the elements corresponding to the peaks comprised the layer. Carbon was detected as a contaminant in the sample.

Fig. 5 shows that the ZnO/PS layers exhibited a dominant diffraction peak at $2\theta = 69.0978°$ corresponding to the PS (1 0 0) layer (Minemoto et al., 2007). The diffraction peak at 34.2398° corresponds to the (0 0 2) plane of the ZnO film, indicating that the ZnO nanocrystalline film was highly oriented along the *c*-axis vertical to the PS layer (Chen and Sun, 2010b). The diffraction peak at 44.3560° is related to Si Carbide (SiC) from the XRD sample holder (Hassan et al., 2011). The sharp diffraction peak from the ZnO film with a weak FWHM of 0.29 [2θ] indicates the high quality of the ZnO film.

The average crystallite size was calculated using the Debye–Scherrer formula as follows (Cullity, 1959):

$$D = \frac{0.9\lambda}{B\cos\theta}, \quad (3)$$

where D is the average grain size, λ is the X-ray radiation wavelength (0.15406 nm), θ is the diffraction Bragg angle and B is the FWHM value in the radians unit. The FWHM value obtained from XRD peak for PS layer was 9.8696×10^{-03} radians and for the ZnO film was 8.0930×10^{-03} radians.

The values of average crystallite size obtained from XRD were 17.06 nm for the PS layer and 17.94 nm for the ZnO film. The decrease in average crystallite size indicated an increase in the porosity of the PS layer (Yon et al., 1987). In addition, the strain (ε_{zz}) of the nanocrystalline ZnO film grown on the PS layer along the *c*-axis can be calculated using the following equation (Tsay et al., 2010):

$$\varepsilon_{zz}(\%) = \frac{c - c_o}{c_o}, \quad (4)$$

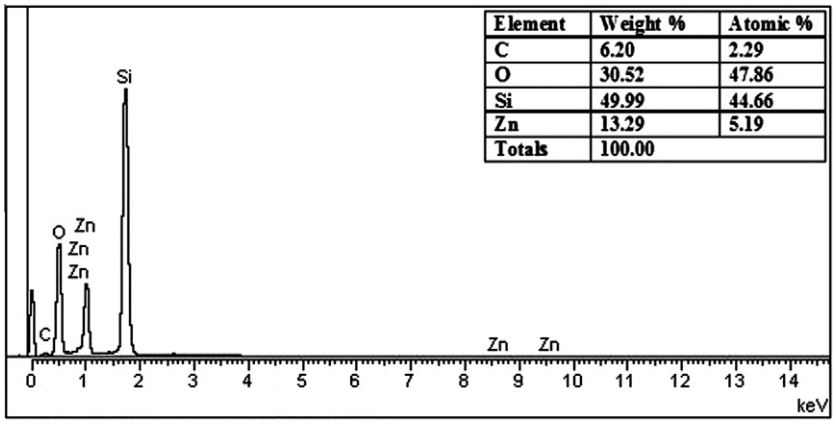

Fig. 4. EDX spectra of ZnO/PS layers.

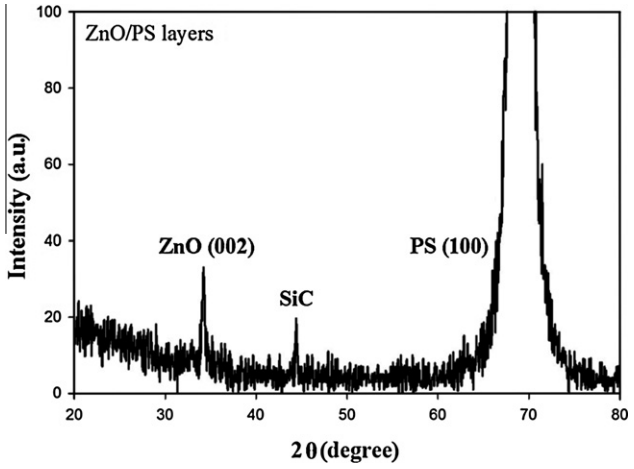

Fig. 5. XRD spectrum of the ZnO/PS layers.

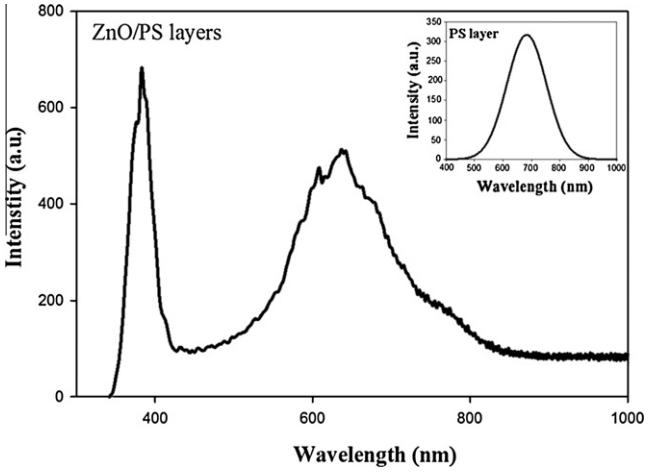

Fig. 6. PL spectra of ZnO/PS layers.

where c is the lattice constant of the strained ZnO film calculated from XRD data, and c_o is the unstrained lattice constant for ZnO. The obtained value of strain is 0.36%. A positive value is associated with tensile strain (Ghosh and Basak, 2004). The low value of the tensile strain revealed that the ZnO nanocrystalline film preferred to grow along the c-axis, and gave evidence of a high-quality crystal resulting from a small lattice mismatch between the ZnO film and the PS (100) layer (9.9%) compared with (39–40.2)% between the ZnO film and c-Si (100) obtained by the sputtering method (Phan and Chung, 2011; Gopalakrishnan et al., 2006).

The PL spectra of the PS and the ZnO/PS layers were measured by a He–Cd excitation laser source at 325 nm at RT (Fig. 6).

The PL spectrum of the PS layer (shown as an inset in Fig. 6) shows a very intense PL emission peak at 683.5 nm, which revealed the good quality of the PS layer (Chen and Chen, 1999).

The left PL peak at 387.5 nm UV emission was caused by the near band edge emission in the wide band gap of the ZnO which resulted from the direct recombination of photogenerated charge carriers (Yu et al., 2009; Umar et al., 2006).

The original value of the PL peak of the bulk ZnO was 367.655 nm (Steiner, 2004). Therefore, the red shift in the PL peak of ZnO film toward a longer wavelength of 387.5 nm was attributed to Zn vacancies in the ZnO energy band gap. Moreover, we believe that contamination of the ZnO/PS layers caused the red shift in the PL peak of the ZnO film (Fig. 6) (Hyunwoo et al., 2006). The right, high-intensity PL peak at 637.5 nm (red emission) is attributed to the PS layer (Liu et al., 2003).

The blue shift in the PL peak of the PS layer toward a shorter wavelength of 637.5 nm is attributed to the quantum confinement effect of electrons in nanosized particles in the PS layer (Chen and Chen, 1999; Hummel et al., 1995). In addition, the observed emission at 637.5 nm is related to the surface oxidation by ZnO deposition (Kayahan, 2010).

The red emission peak for the PS layer containing a shoulder peak of 605 nm (yellow orange emission) in the visible (VIS) region is related to the high number of intrinsic structural defects resulting from Zn vacancies (Jayakumar et al., 2010).

As a result of the high porosity of the PS layer, the blue shift in the PL peak is possible and the high intensity of the strong red emission will occur from the PS layer (Umar et al., 2006; Liu et al., 2003; Prabakaran et al., 2008). In other words, in low-dimensional structures, the probability of the recombination of electrons and holes will be higher, leading to an increase in optical confinement energy and, finally, an increase in photo-conversion efficiency (Wu et al., 2000).

Raman spectra of all layers were measured by an Argon–Ion excitation laser source at 514.5 nm at RT (Fig. 7). A sharp solid line was formed in the c-Si sample spectrum with an FWHM of 3.0 cm^{-1} at 521 cm^{-1} because of the scattering of first-order phonons (Liu et al., 2003).

The penetration depth of the Argon–Ion laser is greater than the thickness of the ZnO film; hence, the spectrum of the PS layer displayed a very strong Raman intensity peak that red-shifted and became broader at 517 cm^{-1} with an FWHM of 8.6 cm^{-1} compared with the c-Si sample. The observed phonon frequency at 302 cm^{-1} was also related to the c-Si substrate in the ZnO/PS layers (Hassan et al., 2011), which has a broadened FWHM and a high intensity compared with the c-Si sample and the PS layer as shown in the inset of Fig. 7.

The formation of the PS layer led to a peak-shift asymmetry and an increase in the peak intensity. This feature of Si nanocrystals is attributed to the quantum confinement of optical phonons in the electronic wave function of Si nanocrystals (Vinod and Lal, 2005).

The ZnO wurtzite hexagonal crystal structure belongs to space group C_{6v}^4 in the group theory with two formula units per primitive cell (Vinod and Lal, 2005). Therefore, the Raman-active zone center for optical phonons is $2A_1 + 2B_1 + 2E_1 + 2E_2$, where A_1 and E_1 symmetry are polar phonon modes with two different frequencies for transverse-optical (TO) and longitudinal-optical (LO) phonons, respectively. The $2B_1$ are silent modes.

The E_2 symmetry is a nonpolar phonon mode with two frequencies: E_2 (high), related to oxygen atoms, and E_2 (low), related to the zinc sub-lattice (Alim et al., 2005). The E_2 (high) mode appears as two bands at 442 and 492 cm^{-1} related to E_2 (high) due to oxygen atoms present after the ZnO deposition (Vinodkumar et al., 2010).

Fig. 8 shows the reflection spectra of all layers compared with the c-Si sample. The PS layer consists of nano-silicon crystals and nano-pores. Therefore, the refractive index was decreased and controlled by the pores with respect to the high porosity, leading to a decrease in reflection (Aspnes et al., 1979). The PS reduced light reflection at wavelengths ranging from 400 to 1000 nm compared with the reflectivity of the c-Si sample.

The lowest effective reflectance was obtained from the ZnO/PS layers, which clearly reduced light reflection and increased light trapping at wavelengths ranging from 400 to 1000 nm compared with the reflectivity of the c-Si sample and PS layer.

The synthesis of ZnO/PS ARC layers in the solar cells enhanced the photo-conversion process with high transparency and increased light absorption in the near-UV/VIS region of the solar spectrum. This is expected to increase the efficiency of solar cells compared with the solar cell without and with a PS ARC layer, respectively (Fig. 9) because the transparency and trapping of the incident radiation resulted from the passivation and heterogeneous properties of the ZnO/PS ARC layers. The solar cells were characterized under a 100 mW/cm^2 illumination condition.

The I–V measurements of the solar cells with ZnO/PS ARC layer confirmed that I_{sc} increased from 14.46 and 33.90 to 35.50 mA/cm^2 and V_{oc} increased from 367.20 and 595.00 to 627.30 mV compared with the solar cell without and with a PS ARC layer, respectively. This leads to an 18.15% increase in conversion efficiency compared with 3.64% and 15.50% for the solar cell without and with a PS ARC layer, respectively.

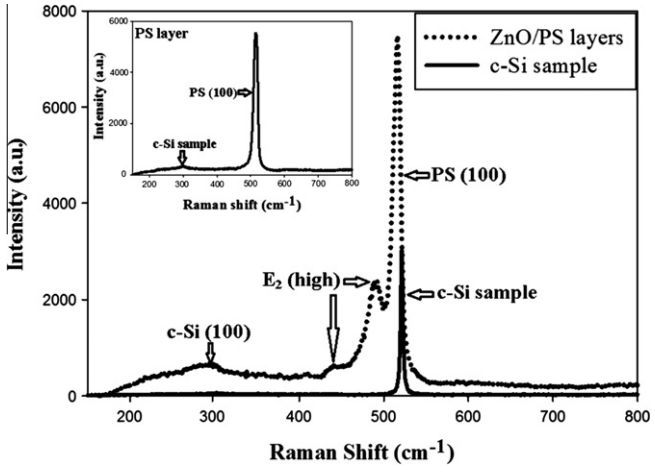

Fig. 7. Raman spectra of ZnO/PS layers compared to the c-Si sample.

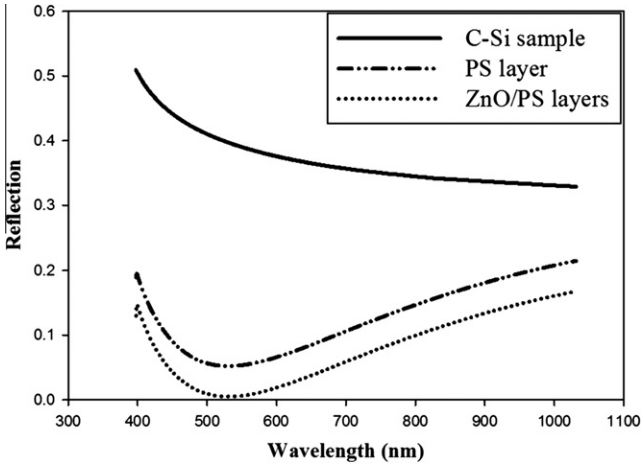

Fig. 8. Reflection spectra of the ZnO/PS layers compared to the c-Si sample and the PS layer.

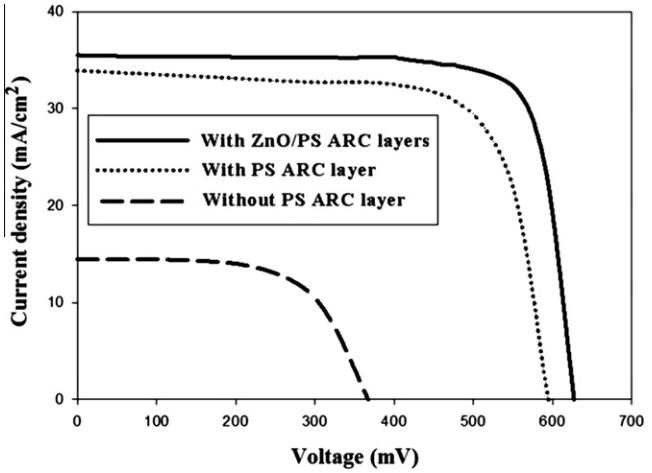

Fig. 9. Current–Voltage curves of solar cells with ZnO/PS ARC layers compared with and without a PS ARC layer.

Table 2
Current–Voltage measurements of solar cells with ZnO/PS ARC layers compared with and without a PS ARC layer.

Solar cells	V_m (mV)	I_m (mA/cm^2)	V_{oc} (mV)	I_{sc} (mA/cm^2)	FF (%)	η (%)
With ZnO/PS ARC layers	550.00	33.00	627.30	35.50	81.50	18.15
With PS ARC layer	503.00	30.82	595.00	33.90	76.40	15.50
Without PS ARC layer	287.90	12.67	367.20	14.46	68.65	3.64

In the present work, the solar cell with ZnO/PS ARC layers displayed increases in (I_{sc}), (V_{oc}), and conversion efficiency compared with the solar cell with and without a PS ARC layer (Table 2).

4. Conclusions

The surface morphology of the PS and ZnO/PS layers was characterized using SEM. Nano-pores with an average diameter of 6.2 nm were produced in the PS layer using the PECE process. This resulted in an increase in porosity up to 91%. The ZnO film was successfully deposited inside the nano-pores of the PS layer along the walls in order for the pores to be partially filled or covered using the RF sputtering system. The ZnO film was highly oriented with the *c*-axis perpendicular to the PS layer. The average crystallite size of the PS and ZnO film was 17.06 and 17.94 nm, respectively. The PL emission peaks proved the nanocrystalline characteristic of the PS layer and the ZnO film. In addition, a high-quality ZnO nanocrystalline film was formed.

The lowest effective reflectance was obtained for the ZnO/PS layers. These layers were found to be an excellent ARC in enhancing and increasing the light conversion efficiency of solar cells to 18.15%, which is close to the efficiency of the commercial solar cells with standard alkaline-textured pyramids and SiN_x single-ARC layer.

Acknowledgment

The authors would like to thank the research university (RU) grant, Universiti Sains Malaysia, and JUST-Jordan and TWAS-Italy Associteship for their support.

References

Alim, K.A., Fonoberov, V.A., Shamsa, M., Balandina, A.A., 2005. Micro-Raman investigation of optical phonons in ZnO nanocrystals. J. Appl. Phys. 97, 124313–124317.

Aspnes, D.E., Theeten, J.B., Hottier, F., 1979. Investigation of effective-medium models of microscopic surface roughness by spectroscopic ellipsometry. Phys. Rev. B 20, 3292–3302.

Bahadur, L., Hamdani, M., Koenig, J.F., Chartier, P., 1986. Studies on semiconducting thin films prepared by the spray pyrolysis technique for photoelectrochemical solar cell applications: Preparation and properties of ZnO. Sol. Energ. Mater. 14, 107–120.

Ben Ranha, M., Bessais, B., 2010. Enhancement of photovoltaic properties of multicrystalline silicon solar cells by combination of buried metallic contacts and thin porous silicon. Sol. Energy 84, 486–491.

Bisi, O., Ossicini, S., Pavesi, L., 2000. Porous silicon: a quantum sponge structure for silicon based optoelectronics. Surf. Sci. Rep. 38, 1–126.

Cai, H., Shen, H., Yin, Y., Lu, L., Shen, J., Tang, Z., 2009. The effects of porous silicon on the crystalline properties of ZnO thin films. J. Phys. Chem. Solids 70, 967–971.

Canham, T.L., 1990. Silicon quantum wire array fabrication by electrochemical and chemical dissolution of wafers. Appl. Phys. Lett. 57, 1046–1048.

Chen, C.H., Chen, Y.F., 1999. Strong and stable visible luminescence from Au-passivated porous silicon. Appl. Phys. Lett. 75, 2560–2562.

Chen, Z., Gao, L., 2006. A facile route to ZnO nanorod arrays using wet chemical method. J. Cryst. Growth 293, 522–527.

Chen, J.Y., Sun, K.W., 2010a. Enhancement of the light conversion efficiency of silicon solar cells by using nanoimprint anti-reflection layer. Sol. Energy Mater. Sol. Cells 94, 629–633.

Chen, J.Y., Sun, K.W., 2010b. Growth of vertically aligned ZnO nanorod arrays as antireflection layer on silicon solar cells. Sol. Energy Mater. Sol. Cells 94, 930–934.

Choi, J.-H., Das, S.N., Moon, K.-J., Kar, J.P., Myoung, J.-M., 2010. Fabrication and characterization of p-Si nanowires/ZnO film heterojunction diode. Solid-State Electron. 54, 1582–1585.

Cullity, B.D., 1959. Elements of X-ray Diffraction. Addison-Wesley, London.

FaŸ, S., Shah, A., 2008. Zinc oxide grown by CVD process as transparent contact for thin film solar cell applications. In: Ellmer, K., Klein, A., Rech, B. (Eds.), Transparent Conductive Zinc Oxide. Springer, Berlin Heidelberg, pp. 235–302.

Fujihara, S., Sasaki, C., Kimura, T., 2001. Crystallization behavior and origin of *c*-axis orientation in sol-gel-derived ZnO:Li thin films on glass substrates. Appl. Surf. Sci. 180, 341–350.

Ghosh, R., Basak, D., 2004. Effect of substrate-induced strain on the structural, electrical, and optical properties of polycrystalline ZnO thin films. J. Appl. Phys. 96, 2689–2692.

Gopalakrishnan, N., Shin, B.C., Lim, H.S., Kim, G.Y., Yu, Y.S., 2006. Comparison of ZnO:GaN films on Si(1 1 1) and Si(1 0 0) substrates by pulsed laser deposition. Phys. B, 756–759 (Amsterdam, Neth.).

Greene, L.E., Law, M., Tan, D.H., Montano, M., Goldberger, J., Somorjai, G., Yang, P., 2005. General route to vertical ZnO nanowire arrays using textured ZnO seeds. Nano Lett. 5, 1231–1236.

Haga, K., Wijesena, P.S., Watanabe, H., 2001. Group III impurity doped ZnO films prepared by atmospheric pressure chemical-vapor deposi-

tion using zinc acetylacetonate and oxygen. Appl. Surf. Sci. 169–170, 504–507.

Harding, G.L., Window, B., Horrigan, E.C., 1991. Aluminium-and indium-doped zinc oxide thin films prepared by DC magnetron reactive sputtering. Sol. Energ. Mater. 22, 69–91.

Hassan, J.J., Hassan, Z., Abu-Hassan, H., 2011. High-quality vertically aligned ZnO nanorods synthesized by microwave-assisted CBD with ZnO-PVA complex seed layer on Si substrates. J. Alloys Compd. 509, 6711–6719.

Hsu, H.-C., Cheng, C.-S., Chang, C.-C., Yang, S., Chang, C.-S., Hsieh, W.-F., 2005. Orientation-enhanced growth and optical properties of ZnO nanowires grown on porous silicon substrates. Nanotechnology 16, 297–301.

Hummel, R.E., Ludwig, M.H., Chang, S.S., 1995. Strong, blue, room-temperature photoluminescence of spark-processed silicon. Solid State Commun. 93, 237–241.

Hyunwoo, L., Lee, E., Soohong, L., 2006. Investigation of nano-porous silicon antireflection coatings for crystalline silicon solar cells. Nano-technology Materials and Devices Conference. NMDC 2006. IEEE, Gyeongju, Korea. pp. 340–341.

Jayakumar, O.D., Sudarsan, V., Sudakar, C., Naik, R., Vatsa, R.K., Tyagi, A.K., 2010. Green emission from ZnO nanorods: Role of defects and morphology. Scr. Mater. 62, 662–665.

Kawakami, M., Hartanto, A.B., Okada, Y.N.T., 2003. Synthesis of ZnO nanorods by nanoparticle assisted pulsed-laser deposition. J. Appl. Phys. 42, 33–35.

Kayahan, Ersin, 2010. White light luminescence from annealed thin ZnO deposited porous silicon. J. Lumin. 130, 1295–1299.

Kim, K.-S., Kim, H.W., 2003. Synthesis of ZnO nanorod on bare Si substrate using metal organic chemical vapor deposition. Phys. B 328, 368–371.

Koshida, N., Koyama, H., 1992. Visible electro- and photoluminescence from porous silicon and its related optoelectronic properties. Mater. Res. Soc. Symp. Proc. 256, 219–222.

Liu, R., Vertegel, A.A., Bohannan, E.W., Sorenson, T.A., Switzer, J.A., 2001. Epitaxial electrodeposition of zinc oxide nanopillars on single crystal gold. Chem. Mater. 13, 508–512.

Liu, Y.L., Liu, Y.C., Yang, H., Wang, W.B., Ma, J.G., Zhang, J.Y., Lu, Y.M., Shen, D.Z., Fan, X.W., 2003. The optical properties of ZnO films grown on porous Si templates. J. Phys. D: Appl. Phys. 36, 2705–2708.

Lu, L., Li, R., Fan, K., Peng, T., 2010. Effects of annealing conditions on the photoelectrochemical properties of dye-sensitized solar cells made with ZnO nanoparticles. Sol. Energy 84, 844–853.

Minemoto, T., Mizuta, T., Takakura, H., Hamakawa, Y., 2007. Antireflective coating fabricated by chemical deposition of ZnO for spherical Si solar cells. Sol. Energy Mater. Sol. Cells 91, 191–194.

Ossicini, S.L., Pavesi, L., Priolo, F., 2003. Light emitting silicon for microphotonics. Springer-Verlag, Berlin Heidelberg.

Pawar, R.C., Shaikh, J.S., Babar, A.A., Dhere, P.M., Patil, P.S., 2011. Aqueous chemical growth of ZnO disks, rods, spindles and flowers: pH dependency and photoelectrochemical properties. Sol. Energy 85, 1119–1127.

Phan, D.-T., Chung, G.-S., 2011. Comparison of ZnO thin films grown on a polycrystalline 3C-SiC buffer layer by RF magnetron sputtering and a sol–gel method. Appl. Surf. Sci. 257, 3285–3290.

Prabakaran, R., Peres, M., Monteiro, T., Fortunato, E., Martins, R., Ferreira, I., 2008. The effects of ZnO coating on the photolumines-cence properties of porous silicon for the advanced optoelectronic devices. J. Non-Cryst. Solids 354, 2181–2185.

Riaz, M., Fulati, A., Amin, G., Alvi, N.H., Nur, O., Willander, M., 2009. Buckling and elastic stability of vertical ZnO nanotubes and nanorods. J. Appl. Phys. 109, 034309–034314.

San Vicente, G., Bayón, R., Germán, N., Morales, A., 2011. Surface modification of porous antireflective coatings for solar glass covers. Sol. Energy 85, 676–680.

Sil, D., Chakrabarti, S., 2010. Photocatalytic degradation of PVC-ZnO composite film under tropical sunlight and artificial UV radiation: A comparative study. Sol. Energy 84, 476–485.

Steiner, T., 2004. Semiconductor nanostructures for optoelectronic applications. Artech House Inc, Norwood.

Tak, Y., Yong, K., 2005. Controlled growth of well-aligned ZnO nanorod array using a novel solution method. J. Phys. Chem. B 109, 19263–19269.

Tsay, C.-Y., Fan, K.-S., Chen, S.-H., Tsai, C.-H., 2010. Preparation and characterization of ZnO transparent semiconductor thin films by sol–gel method. J. Alloys Compd. 495, 126–130.

Ueda, K., Nakato, Y., Tsubomura, H., 1988. Efficient and stable solar to chemical conversion with n+-p junction crystalline silicon electrodes having textured surfaces. Sol. Energ. Mater. 17, 37–46.

Umar, A., Karunagaran, B., Suh, E.-K., Hahn, Y.B., 2006. Structural and optical properties of single-crystalline ZnO nanorods grown on silicon by thermal evaporation. Nanotechnology 17, 4072–4077.

Vasanelli, L., Valentini, A., Losacco, A., 1987. Preparation of transparent conducting zinc oxide films by reactive sputtering. Sol. Energ. Mater. 16, 91–102.

Vinod, P.N., Lal, M., 2005. Surface and optical characterization of the porous silicon textured surface for application in photovoltaics. Photovoltaic Specialists Conference, 2005. Conference Record of the Thirty-first IEEE, 3–7 January 2005, pp. 1135–1138.

Vinodkumar, R., Navas, I., Chalana, S.R., Gopchandran, K.G., Ganesan, V., Philip, R., Sudheer, S.K., Mahadevan Pillai, V.P., 2010. Highly conductive and transparent laser ablated nanostructured Al: ZnO thin films. Appl. Surf. Sci. 257, 708–716.

Vitanov, P., Kamenova, M., Tyutyundzhiev, N., Delibasheva, M., Goranova, E., Peneva, M., 1997. High-efficiency solar cell using a thin porous silicon layer. Thin Solid Films 297, 299–303.

Wong, E.M., Searson, P.C., 1999. ZnO quantum particle thin films fabricated by electrophoretic deposition. Appl. Phys. Lett. 74, 2939–2941.

Wu, X.L., Xiong, S.J., Fan, D.L., Gu, Y., Bao, X.M., 2000. Stabilized electronic state and its luminescence at the surface of oxygen-passivated porous silicon. Phys. Rev. B 62, 7759–7762.

Yae, S., Kobayashi, T., Kawagishi, T., Fukumuro, N., Matsuda, H., 2006. Antireflective porous layer formation on multicrystalline silicon by metal particle enhanced HF etching. Sol. Energy 80, 701–706.

Ye, Z.Z., Lu, J.G., Zhang, Y.Z., Zeng, Y.J., Chen, L.L., Zhuge, F., Yuan, G.D., He, H.P., Zhu, L.P., Huang, J.Y., Zhao, B.H., 2007. ZnO light-emitting diodes fabricated on Si substrates with homobuffer layers. Appl. Phys. Lett. 91, 113503–113505.

Yon, J.J., Barla, K., Herino, R., Bomchil, G., 1987. The kinetics and mechanism of oxide layer formation from porous silicon formed on p-Si substrates. J. Appl. Phys. 62, 1042–1048.

Yoo, J., 2010. Reactive ion etching (RIE) technique for application in crystalline silicon solar cells. Sol. Energy 84, 730–734.

Yu, C.-F., Sung, C.-W., Chen, S.-H., Sun, S.-J., 2009. Relationship between the photoluminescence and conductivity of undoped ZnO thin films grown with various oxygen pressures. Appl. Surf. Sci. 256, 792–796.

Yun-Ju, L., Ruby, D.S., Peters, D.W., Mckenzie, B.B., Hsu, J.W.P., 2008. ZnO Nanostructures as efficient antireflection layers in solar cells. Nano Lett. 8, 1501–1505.